https://doi.org/10.5194/egusphere-2023-947
Preprint. Discussion started: 15 May 2023

Statistical Analysis on the Estimations of Solid Hydrometeors Growth Zones and Their Weather Conditions Using Radar Spectrum Width

Sung-Ho Suh[1*], Woonseon Jung[2], Hong-Il Kim[1], Eun-Ho Choi[1], and Jung-Hoon Kim[3]

Institutional addresses:

[1]Flight Safety Technology Division, NARO Space Center, Korea Aerospace Research Institute (KARI), 508 Haban-ro, Bongrae-myeon, Goheung-gun, Jeollanam-do, Republic of Korea

[2]Research Applications Department, National institute of meteorological sciences, 33, Seohobuk-ro, Seoqwipo-si, Jeju-do, 63568, Republic of Korea

[3]School of Earth and Environmental Sciences, Seoul National University, Seoul 08826, Republic of Korea

*Corresponding author: Dr. Sung-Ho Suh (suhsh@kari.re.kr)

Keywords: Spectrum width, Aerodynamic properties, Solid Hydrometeors, Weather radar, Dendritic Growth Zone (DGZ), Needle Growth Zone (NGZ), Growth Zone Determination Algorithm (GZDA).

https://doi.org/10.5194/egusphere-2023-947
Preprint. Discussion started: 15 May 2023

Abstract

This study analyzes the correlation between hydrometeor type and radar spectrum width (σ_v) according to wind speed that can occur the atmospheric disturbances such as turbulence and wind shear. The σ_v zones shown as peak values were identified only in stratiform precipitation and they are highly related to the hydrometeor growth zones. Statistical analysis was performed for eight precipitation cases under various conditions (precipitation type, season), focusing on the Dendrite Growth Zone (DGZ) and the Needle Growth Zone (NGZ), where Dendrite (DN) and Needle (NE) type snowflakes are dominant, respectively. They were determined by the Growth Zone Determination Algorithm (GZDA) that was proposed in this study.

The intensity of the σ_v depends on atmospheric conditions (i.e., wind speed) and season (i.e., temperature). The high σ_v and negative relationship with the differential radar reflectivity (Z_{DR}) in the DGZ for all cases is consistent with the aerodynamic properties of DN. As the range of σ_v was larger than that of Z_{DR}, it was confirmed that the dependence of σ_v according to atmospheric conditions is significant. Contrastingly, the NGZ had a low σ_v and weak σ_v-Z_{DR} negative relationship with a narrow range of σ_v, which is consistent with the aerodynamic properties of NE. The lower cross-correlation coefficient (ρ_{hv}) in the DGZ than that in the NGZ implies that the irregularities (particle shape and aerodynamics features) of DN were more pronounced than those of NE.

Finally, as the altitudes of two growth zones were determined by temperature, the possibility of estimating sub-zero temperature by GZDA was confirmed.

https://doi.org/10.5194/egusphere-2023-947
Preprint. Discussion started: 15 May 2023

1. Introduction

Naturally formed ice crystal has various shapes. The International Commission on Snow and Ice describes seven ice crystal types: needles, columns, capped columns, plates, stellar crystals, spatial dendrites, and irregular forms (Mason, 1971). Libbrecht (2006) mentioned the field guide to the 35 type of snowflakes by 35 type with irregular snowflake. Hydrometeor identification helps in various fields such as I) remote sensing, in terms of quantitative precipitation estimation (e.g., Giangrande and Ryzhkov, 2008; Kennedy and Rutledge, 2011; Bechini et al., 2013), II) understanding the mechanisms of lightning formation (e.g., Ribaud et al., 2016), and III) aviation safety (e.g., Williams et al., 2011; 2013).

The solid hydrometeor formations that develop are determined by the water vapor pressure and atmospheric temperature (T). Ice crystals can develop with fine dust particles at T > -40 °C. The dendrites growth zone (DGZ) can be found at an altitude (H) where T range between -20 °C < T < -10°C, while the needles growth zone (NGZ) can be found at H where between -5 °C < T < 0 °C (Nakaya and Terada, 1935). Aircraft icing, which causes severe aviation problems, generally occurs at the altitude at which supercooled water droplets are present, corresponding to the range of -20 °C < T < 0 °C (Gent et al., 2000; Politovich et al., 2003). This indicates that the icing phenomenon may occur between two growth zones (GZs); thus, identifying GZs during flight is crucial for aviation safety.

The physical condition of the particle (i.e., size, shape, and density), as well as atmospheric condition (i.e., dynamic viscosity, atmospheric density), influences particle movements (i.e., vibration, orientation, and tumbling). Previous studies (e.g., Nakaya and Terada, 1935; Willmarth et al., 1964; List and Schemenauer, 1971; Ji and Wang, 1991; Wang and Ji, 1997; 2000; Wang, 2002; Hashino et al., 2014; 2016) have explained that particle behavior depends on shape, implying that a particle can exhibit various motions even under the same atmospheric condition. This further implies that radar velocity spectrum width (σ_v) may also depend on the shape and this assumption can be resolved if high

https://doi.org/10.5194/egusphere-2023-947
Preprint. Discussion started: 15 May 2023

spatiotemporal measurements exist in a zone where each hydrometeor is homogenized (i.e., GZs).

Dual-polarization (dual-pol) weather radar supports high spatiotemporal measurements for analyzing information on the sizes, shapes, and movements of various hydrometeors. Weather radar has an excellent performance detecting and analyzing solid hydrometeors (e.g., Vivekanandan et al., 1994; Ryzhkov et al., 1998; Wolde and Vali, 2001; Williams et al., 2011; 2013). Therefore, the compositions in the DGZ (Kennedy and Rutledge, 2011; Andrić et al., 2013; Bechini et al., 2013; Suh et al., 2023) can be explained by these radar products. Suh et al. (2023) demonstrated that the major radar products with which to analyze GZs include their differential radar reflectivity (Z_{DR} in dB), cross-correlation coefficient (ρ_{hv}), and velocity spectral width (σ_v in m s^{-1}). The differential radar reflectivity explains the particle's oblateness (e.g., oblate, prolate). In contrast, the composition of hydrometeor types and orientation of particles within the radar observation bin can be described by ρ_{hv}. The radar velocity spectrum width, one of the major products obtained by Doppler weather radar, represents the deviation in target movement within the observed resolution volume (Brewster and Zrnić, 1986; Doviak, 2006; Zhang et al., 2009).

Researchers have attempted to find the relationship between turbulent motion and σ_v (Labitt et al., 1981; Knupp and Cotton, 1982; Hocking, 1985; Istok and Doviak, 1986; Jacoby-Koaly et al., 2002; Melnikov and Doviak, 2009). Zhang et al. (2009) described the eddy dissipation rate (EDR) derived by σ_v from 14 cases with different weather conditions observed in the Hong Kong airport and evaluated by aircraft measurements. Recently, Kim et al. (2021) suggested a new technique to estimate the σ_v-based EDR using a lognormal mapping algorithm. The estimates show a high correlation with the quick access recode data supported by the commercial aircraft and the EDR calculated by numerical weather prediction. Suh et al. (2023) suggested that σ_v can depend on the hydrometeor type based on the features of radar products for GZs, which has been affirmed through simulations for dendrite (DN) and needle (NE) types of snowflakes. However, they explained the need for further analysis as their

https://doi.org/10.5194/egusphere-2023-947
Preprint. Discussion started: 15 May 2023

study I) considered only two winter precipitation cases and II) their GZs were extracted qualitatively.

As a follow-up to the study of Suh et al. (2023), this study suggests that representative features of σ_v and dual-pol radar variables according to the atmospheric conditions [i.e., T, wind speed (v in m s^{-1})] in GZs improve the practicality of the present results based on statistical analysis using eight precipitation cases with various conditions (i.e., season, precipitation type), and a quantitative approach through a Growth Zone Determination Algorithm (GZDA). In addition, the possibility of estimating T above freezing levels with weather radar was examined by the GZDA. The remainder of this paper is presented as follows: Section 2 provides details on the data and instruments, including the structure of the GZDA. The results of the radar products extracted by the GZDA and their performance are investigated in Section 3, with a discussion of said results found in Section 4, while the conclusions of this study are presented in Section 5.

https://doi.org/10.5194/egusphere-2023-947
Preprint. Discussion started: 15 May 2023

2. Data and Methods

2.1. Analysis instrument and data

The Yongin Testbed dual-pol weather radar (YIT) was used to analyze the features of GZs (Fig. 1). It has been operated by the Weather Radar Center, under the Korean Meteorological Administration (KMA), from July 2014 until the present. The Enterprise Electronics Corporation manufactured the YIT with coverage of up to 240 km and an S-band (2.88 GHz) transmission frequency. Specifications regarding the YIT are presented in Table 1.

The cases analyzed in Suh et al. (2023) were limited to winter stratiform precipitation, while the scope of the present study was expanded to examine the radar products in GZs for eight precipitation cases which can be divided into I) winter stratiform precipitation, and II) non-winter precipitation. Non-winter precipitation cases were subdivided into stratiform and convective types (Table 2). They are expressed as abbreviations to describe the characteristics of cases with various conditions intuitively. The first letter of the abbreviation means the precipitation type [Stratiform (S) and Convective (C)], and the second letter means the season [Spring (P), Summer (S), and Winter (W)]. The last digit is the number indicating the case. From the PPI for the lowest elevation angle (θ), if there is a significant cell that satisfies the radar reflectivity (Z_H) > 40 dBZ within 1km of vertical altitude from the ground or that satisfies Z_H > 45 dBZ within 250 km radar slant range, it was considered as convective precipitation. The research cases selected satisfied the following conditions: I) the precipitation occurred for at minimum over three hours at the YIT site, and II) the vertical depth of Z_H in a precipitation system higher than 5 dBZ exceeded 2 km (Fig. 2).

Meteorological information was obtained from the mesoscale model (MSM) reanalysis data to analyze the radar products according to atmospheric conditions in GZs. The MSM provided by the Japanese Meteorological Agency supports meteorological parameters for sixteen pressure altitudes. As

https://doi.org/10.5194/egusphere-2023-947
Preprint. Discussion started: 15 May 2023

this reanalysis data has a better spatial resolution of pressure altitudes increases as it is closer to the ground, it is useful to interpret the atmospheric information for altitudes below the middle level (500 hPa).

2.2. Analysis strategies

2.2.1. QVP

The quasi-vertical profile (QVP) technique proposed by Ryzhkov et al. (2016) was applied to define and analyze the GZs. The QVP is a computationally efficient scheme because it can be calculated with only one sweep. Radar products in QVP are obtained by azimuth averaging and are expressed in a time-height format. Moreover, this technique helps analyze the features of hydrometeors (Ryzhkov et al., 2016). The slant ranges at the three target elevation angles (19°, 17.3°, and 16.4°) for the altitude of 12 km without consideration of the curvature of the earth are 36.85 km, 40.12 km, and 42.50 km, respectively. A slant range of approximately 2.5 km from YIT is considered a dead zone, corresponding to H of approximately 0.8 km at $\theta = 19°$, the highest elevation level in the selected cases.

2.2.2. GZ Determination Algorithm (GZDA)

This study determined the GZ for several precipitation cases, including various seasons, through quantitative criteria in a deductive approach to analyze the statistical characteristics of the GZs. A total of 5 stages were conceived in the GZ Determination Algorithm (GZDA) to identify GZs for all precipitation cases (Fig 3).

STAGE 1 (Pre-processing): Firstly, the QVP was created and then the median value of σ_v (σ) and its variation ($d\sigma$) for each vertical window channel in the whole analysis periods were calculated. After

https://doi.org/10.5194/egusphere-2023-947
Preprint. Discussion started: 15 May 2023

that σ and dσ are smoothed for ±1 vertical window channel to define the peak of dσ (κ) and its altitude (H_κ).

STAGE 2 (κ and H_κ determination): To remove the noise in κs, only one κ which corresponds to the extreme value in ±2 vertical window channel was selected.

STAGE 3 (Freezing level considerations): The region of interest in this study was an altitude at which the temperature is below freezing. κ can be found not only on the freezing layer but also on the melting layer (ML), negatively affecting the correct determination of σ and dσ. Thus, κ was identified and removed from the bottom of the ML to the ground before procedures were implemented on the freezing level, which was the target of analysis. This procedure for the unfreezing level should be prioritized since a minimum κ may be found at the bottom of the ML rather than near the bottom of the NGZ.

STAGE 4 (GZ determination): κ that satisfied the characteristics of interest shown in GZs were selected and defined as their boundary. To accomplish this, extreme values of σ that can be considered as the core of each GZ within the freezing level were chosen. Then, the altitudes where the minimum and maximum values of σ ($H_{\sigma1}$ and $H_{\sigma2}$, where $H_{\sigma1} < H_{\sigma2}$) exist, representing the cores of the NGZ and the DGZ, respectively, were found. This means that the peak values of κ are matched to the boundary altitudes of GZs. The altitudes at the bottom and top of the DGZ (the NGZ) have the local maxima (minima) and the local minima (maxima) of κ, respectively. After the two procedures described above were complete, the four nearest H_κs (H_{N1}, H_{N2}, H_{D1}, and H_{D2}) from the peak value of σ could be designated as the boundary list. These four points have to be satisfied the following conditions: I) $H_{N1} \leq H_{\sigma1} \leq H_{N2}$, and II) $H_{D1} \leq H_{\sigma2} \leq H_{D2}$.

STAGE 5 (Post-process): The final step was to determine whether the selected GZs met realistic conditions and to supplement the results that were not resolved in Stage 4. When only the bottom of

https://doi.org/10.5194/egusphere-2023-947
Preprint. Discussion started: 15 May 2023

the DGZ (H_{D1}) was chosen as the boundary list for DGZ due to the limitations of the radar observation strategy, the echo top height (H_T) was chosen as the top of the DGZ (H_{D2}). In addition, since it is rare for the thickness of GZ to exceed 1.5 km in natural conditions, the GZs that satisfies this condition may unreliable, so it was excluded. A detailed description of the algorithm with the overall procedure was summarized in Figure 5.

2.3. Data quality control

Initially, a fuzzy logic algorithm was applied (Gourley et al., 2007) to radar products to remove non-meteorological targets. The σ_v was removed when it satisfied a signal-to-noise ratio (SNR) condition where SNR < 20 dB because σ_v shows a large variance for lower SNRs (Zhang et al., 2009). The following three additional QC procedures for QVP data were performed after the aforementioned QC procedures: I) the radar product in PPI was removed if the number of data points where $Z_H > 5$ dBZ was less than 20 % of the total number of azimuths at the i^{th} radar bin, and II) the QVP for $Z_H \leq 5$ dBZ was selected, III) the calibrated Z_{DR} was applied because the projected area of the target depends on the line of sight. The Z_{DR} calibration suggested by Ryzhkov et al. (2005) was introduced as follows,

$$Z_{DR}(\theta) = \frac{Z_{DR}(0)}{[Z_{DR}(0)^{1/2} sin^2\theta + cos^2\theta]^2}$$

The radar elevation angles for QVP considered in this study are θ = 16.4°, 17.3°, and 19.0°, and the calibrated Z_{DR} for these θ are 0.916Z_{DR}, 0.906Z_{DR}, and 0.887Z_{DR} for θ=0°, respectively.

https://doi.org/10.5194/egusphere-2023-947
Preprint. Discussion started: 15 May 2023

3. Results

3.1. Analysis of QVPs

3.1.1 QVP for various conditions of precipitation cases

The features of QVP-based dual-pol radar variables are classified into the type of precipitation (stratiform and convective precipitation). Seasonal factors can also subdivide the profile pattern for stratiform precipitation. Figure 4 presents a representative case to explain the common feature of dual-pol radar products for the non-winter stratiform precipitation case selected in this study. The following common features can be identified from the QVP for the non-winter stratiform precipitation.

First, the altitude of melting layer can be confirmed at H > 1 km where the weather radar can clearly detect height. High Z_H, Z_{DR}, and low ρ_{hv} can be found in the ML due to the melting of solid hydrometeors (Trömel et al., 2017). In addition, weak Z_H and ρ_{hv} appear in the upper layer of the ML, while high Z_H and ρ_{hv} appear in the lower layer of the ML due to the increase in the dielectric constant and the uniformity of particle shape. A low Z_{DR} appears near the top of the ML and increases with H. Further, in the layer of a degree above zero, a higher Z_{DR} than near the top of the ML can be found, which corresponds to a negative relationship between Z_H-Z_{DR} (i.e., solid hydrometeor), indicating a spherical hydrometeor (i.e., raindrop) with high Z_H (i.e., high dielectric constant). There are no remarkable features in σ_v except for a weak increase in the ML.

By contrast, stratiform precipitation in winter can have only solid hydrometeors in the whole system since strong vertical convection, which can transport supercooled water droplets to the upper layers, have not developed (Fig. 5). Stratiform precipitation in winter has comparable characteristics to those of the non-winter season. Firstly, there are no ML; thus, the entire precipitation system matches the features in the upper layer of ML. Secondly, two σ_v zones in the freezing level can be found, which are distinctly developed on H where temperatures are -5 ℃ and -15 ℃, respectively.

https://doi.org/10.5194/egusphere-2023-947
Preprint. Discussion started: 15 May 2023

3.1.2 GZ determination in QVP

The vertical profiles of σ_v to which GZDA was applied for various precipitation cases are shown in Figure 6. All GZs were determined correctly for the stratiform precipitation group, and there were no GZs determined by GZDA for precipitation cases classified as a convective type.

In the vertical profile of σ_v for stratiform precipitation in winter, extreme values of σ can be confirmed, which were statistically significant for cases of SW3 and SW4. Minimum and maximum values of σ are observed for NGZ and DGZ, respectively, in all precipitation cases presented from GZDA. In the case of SW1-4, it was found that the top of the DGZ, which was not identified due to the characteristics of the case formed at a low altitude, clearly appeared in SP7. Through this, it can be confirmed in the case of SP7 that the σ_v in the freezing level is not proportional to the altitude. The maxima of σ is found around $3 < H$ (km) < 4 and $H = 4.5$ km for cases in the spring and summer seasons, respectively, but it matches the altitude of the ML. Moreover, the vertical profiles of σ_v in these cases had a vertically symmetrical pattern centered on the ML. In addition, there were κ in convective precipitation cases determined by GZDA, but GZs are not presented since the κ did not satisfy the conditions of the algorithm. There are minima of $d\sigma_v$ in the GZ transition region for stratiform precipitation cases but it not shown in figure since it is removed by the algorithm (Fig. 7). Still, no minima of $d\sigma_v$ was observed in the region between 2nd and 3rd of the boundary list that can be expected as a transition region of GZ for convective precipitation cases (CP6 and CS8) even though they have four κs.

3.2. Features of dual-pol variables in GZs

https://doi.org/10.5194/egusphere-2023-947
Preprint. Discussion started: 15 May 2023

3.2.1 Dominant features in GZs

The characteristics of the dual-pol weather radar variables in the σ_v zones defined from the GZDA were different from those obtained in the altitudes where T = -15 °C and -5 °C, which corresponds to the potential area of DGZ and NGZ for the stratiform precipitation case. The weather information provided from the MSM reanalysis data was used. To select the possible area of GZs for convective precipitation cases that were not defined by the GZDA, ranges of ±0.3 km (DGZ) and ±0.1 km (NGZ) from the H where T = -5 °C and -15 °C were considered. The potential range of the GZs were defined by the average range of the GZs identified in this study, but that of the NGZ were strictly defined relatively narrow in order not to include the ML.

For the DGZ, Z_{DR} for stratiform precipitation in winter was widely distributed around the positive values (Fig. 8). Contrastingly, stratiform precipitation in the spring, and especially convective precipitation, had a concentrated distribution with a narrow modal range of $0.4 < Z_{DR}$ (dB) < 0.7. The cases of SW1 and SW2 showed a high Z_{DR}, with a modal Z_{DR} of 1 dB due to a strong Z_{DR} column. By contrast, the cases of SW3 and SW4 had the lowest Z_{DR} distribution among all cases, with modal values ranging from $0.2 < Z_{DR}$ (dB) < 0.3. In terms of ρ_{hv}, stratiform precipitation in winter for cases other than SW2 showed a wide and gentle distribution with a mode of $0.976 < \rho_{hv} < 0.986$. Contrarily, those in non-winter precipitation had a relatively high mode ($0.983 < \rho_{hv} < 0.990$) with a concentrated distribution. The distribution of σ_v had a negative relationship with that of Z_{DR}, which is consistent with Suh et al. (2023). SW3 and SW4, which had a lower Z_{DR}, had the highest modal value, at about $\sigma_v = 1.2$ m s^{-1}, while SW1 and SW2, which had a higher Z_{DR}, showed relatively low modes at about $0.5 < \sigma_v$ (m s^{-1}) < 0.8. The distribution of σ_v for non-winter precipitation cases also showed a negative relationship with Z_{DR}, similar to the winter cases.

The Z_{DR} in the NGZ showed a similar pattern to that of the DGZ (Fig. 9). The mode of Z_{DR} in SW3

https://doi.org/10.5194/egusphere-2023-947
Preprint. Discussion started: 15 May 2023

and SW4 was negative, while all other cases had positive values. In contrast, ρ_{hv} and σ_v in the NGZ showed noticeably different distributions from those in the DGZ. First, the distribution of ρ_{hv} was concentrated with a mode of $0.930 < \rho_{hv} < 0.996$ for all cases except for SW3 and SW4, which showed gentle distributions centered on $\rho_{hv} = 0.985$. In addition, it is characterized by having the highest ρ_{hv} among all cases centered on $\rho_{hv} = 0.995$ in non-winter precipitation. These tendencies are also confirmed in σ_v. The case of SW3 and SW4 had gentle distributions of σ_v, with a mode of 0.70 m s^{-1}, while all other cases showed a concentrated distribution with various modes ranging from $\sigma_v = 0.4$ m s^{-1} to 0.64 m s^{-1}.

3.2.2 Relationships of dual-pol variables

Correlation analysis was performed to interpret the relationship between the dual-pol radar variables and σ_v which showed a dependence on precipitation type for each case in GZs (Fig. 10). Z_{DR}-σ_v in the DGZ showed a negative relationship for all cases (Fig. 10a). A high σ_vs of 1.2 m s^{-1} in SW3 and SW4 were found, where σ_v gradually decreased as Z_{DR} increased in other cases. Z_{DR}-σ_v had various relationships for each case, but generally, their distribution did not correlate. SW2 and SW3 had a positive correlation for Z_{DR}-σ_v, but in the case of SW2, correct linear regression was not performed since most of the data points were concentrated in $Z_{DR} \sim 1$ dB. In the case of SW3, the distribution of Z_{DR}-σ_v did not correlate. ρ_{hv} did not show a significant correlation with σ_v, but Z_{DR} showed a common trend of inverse proportion to ρ_{hv} in all cases.

The averaged Z_{DR}- σ_v of each case have a negative relationship, and the variation range of σ_v is higher than that of Z_{DR} (Fig. 10b). Additionally, ρ_{hv} showed a negative relationship with σ_v. Remarkably, the cases SW3 and SW4 displayed the lowest ρ_{hv} and the highest σ_v. Z_{DR}- σ_v had a linear distribution and showed a remarkable correlation, with a root mean square error (RMSE) = 0.05 m s^{-}

https://doi.org/10.5194/egusphere-2023-947
Preprint. Discussion started: 15 May 2023

[1], in stratiform precipitation in winter. On the other hand, in all stratiform precipitation cases, Z_{DR}-σ_v had a relatively low correlation of RMSE = 0.11 m s^{-1}. They had a significantly different distribution in convective precipitation from stratiform precipitation in winter. Average Z_{DR}-σ_v values for SP7 were located in between stratiform precipitation in winter and convective precipitation.

In the case of the NGZ, Z_{DR}-σ_v had a relatively weak negative correlation for all cases (Fig. 10c). The variation range in Z_{DR} was broader than that observed in the DGZ, ranging from -0.5 dB – 3 dB. Also, ρ_{hv} showed a negative correlation with both Z_{DR} and σ_v. There was a negative Z_{DR}, while ρ_{hv} increased overall (ρ_{hv} > 0.98) in the NDZ, compared to the DGZ. In contrast, Z_{DR}-σ_v for each case had a positive relationship except for convective precipitation, and their slope tended to depend on the Z_{DR} for each case. The positive correlation between Z_{DR} and σ_v tended to increase as the Z_{DR} for each case decreased.

The averaged Z_{DR}-σ_v of each case, for all cases in the NGZ had a relatively weaker negative relationship than that in the DGZ (Fig. 10d). There was a remarkable variance in Z_{DR} compared to that of σ_v, differing from what is observed in the DGZ. The high σ_v found in SW3 and SW4 also displayed a considerable variation in σ_v, while SW1 and SW2 had a low σ_v and a large variation in Z_{DR}. The pattern in ρ_{hv} and σ_v corresponded to that of the DGZ, while the overall averaged ρ_{hv} was higher than that of the DGZ. A linear distribution with a striking correlation of RMSE = 0.03 m s^{-1} was shown for both stratiform precipitation in winter and total stratiform precipitation cases. In addition, a significant difference from the DGZ is that the averaged σ_v-Z_{DR} for convective precipitation is also located quite close to the regression lines for those of stratiform precipitation.

The maturity of GZs is related to the ratio of dominant solid hydrometeor within each GZ. It appears to have an inverse relationship with ρ_{hv}, and the lower ρ_{hv} in the DGZ compared to NGZ was found (Suh et al., 2023). The maturity of GZs can be indirectly explained by the difference in aerodynamic

https://doi.org/10.5194/egusphere-2023-947
Preprint. Discussion started: 15 May 2023

characteristics (i.e., σ_v) between the core of GZ and that of boundaries ($d\sigma_{MAX}$). Overall, $d\sigma_{MAX}$ showed a pattern inversely proportional to ρ_{hv} (Fig. 11). There is a negative correlation between $d\sigma_{MAX}$ and σ_v. For the range of $\sigma_v > 0.7$ m s^{-1}, only stratiform precipitation is confirmed, and conversely, for the range of $\sigma_v < 0.7$ m s^{-1} where convective precipitation dominates, the condition of $d\sigma_{MAX} < 0.03$ was confirmed**.** The negative relationship between $d\sigma_{MAX}$ and ρ_{hv} was more apparent in the NGZ. The NE had the highest $d\sigma_{MAX}$ (0.13 and 0.21) among all cases in SW3 and SW4, where the averaged Z_{DR} was negative value. $d\sigma_{MAX}$s for stratiform precipitation in all cases except for SW3 and SW4 was found to be between 0.08 and 0.11, while convective precipitation had a low $d\sigma_{MAX}$ of less than 0.04.

3.3. Characteristics of dual-pol radar variables in GZs with atmospheric condition

The dual-pol radar variables are determined by the maturity of GZs. In addition, atmospheric disturbance affects the orientation of the hydrometeor, which increases σ_v and decreases ρ_{hv}, thus influencing Z_{DR}. Consequently, $d\sigma_{MAX}$ can depend on aerodynamic conditions. It was confirmed by the relationship between v and σ_v in GZs.

The σ_v has a positive relationship with v for all cases in the DGZ (Fig. 12). In particular, it displays a marked correlation with an RMSE = 0.14 m s^{-1} for only stratiform precipitation in winter. SP7 showed a relatively weak σ_v of 0.76 m s^{-1} despite having a condition of strong v of about 26 m s^{-1}. Accordingly, the linear regression for all stratiform precipitation cases was less correlated (RMSE = 0.25 m s^{-1}) than for stratiform precipitation in winter (RMSE = 0.14 m s^{-1}). In addition, convective precipitation showed a relatively weak σ_v of $0.48 < \sigma_v$ (m s^{-1}) < 0.66 despite a relatively strong v of more than 17 m s^{-1}. SP7 was not included in the σ_v-v relationship for stratiform precipitations because of the lower σ_v even though the strongest v (26 m s^{-1}) among the whole case. This supports the explanation that seasonal conditions influence the developmental characteristics of GZs. In addition, CS8 showed the lowest

https://doi.org/10.5194/egusphere-2023-947
Preprint. Discussion started: 15 May 2023

correlation as it showed the lowest σ_v (0.5 m s^{-1}) within the same v range. NGZ was confirmed to be uncorrelated to σ_v-v, as suggested by Suh et al. (2023). Interpretable correlations were not identified for stratiform and convective precipitation since averaged σ_vs for all cases except for SW3, and SW4 can be found in 0.43 < σ_v (m s^{-1}) < 0.67 regardless of v.

4. Discussion

The growth rate of each hydrometeor type depends on the condition of T and Water vapor pressure (Nakaya and Terada, 1935). Water vapor pressure depends on atmospheric pressure, meaning that the development of GZs can be determined by altitude. That's why the intensity of σ_v zone shown in the present study appear to be inverse proportional to the altitude of GZ. The intensity of the σ_v zone in seasonal stratiform precipitation clearly verified this. Although there was more substantial average v (26 m s^{-1}) compared to higher that of winter stratiform precipitation, SP7 showed relatively low σ_v (~0.76 m s^{-1}) because the DGZ for the stratiform precipitation in spring had a higher altitude (5.4 < H (km) < 5.9) than that of the winter season (2.6 < H (km) < 4.1). Nevertheless, the atmospheric temperature where each GZ was found remains consistent regardless of the intensity of σ_v and its altitude. It implies that as GZ altitude depends on atmospheric temperature, it suggests that radar-based sub-zero T estimation from GZDA might be possible. The GZDA-based statistical analysis presented here confirmed that stratiform precipitations in winter satisfied the temperature conditions, with -10 < T (°C) < -16 and 0 < T (°C) < -5 in both the DGZ and the NGZ, respectively (Fig. 13). Once GZs have been determined, a transition area between the GZs can be identified. This implies that the real-time estimation of T for every 5 °C class interval from 0 °C to -15 °C by the weather radar will is possible. It is expected that GZDA can be used for the purpose of flight safety since the layer where GZ can develop is matched with the layer at which aircraft icing can occur.

https://doi.org/10.5194/egusphere-2023-947
Preprint. Discussion started: 15 May 2023

As explained in the introduction section, EDR can be estimated from σ_v, representing the variation of particle motion within the observation volume (e.g., Zhang et al., 2009; Kim et al., 2021). Suh et al. (2023) suggested the possibility that σ_v depended on hydrometeor types, which was confirmed in this study. This means that σ_v (EDR) can be varied by the hydrometeor types under the same atmospheric conditions. As a result, the following two improvements are suggested, I) EDR correction: First, the correction of σ_v-based EDR would be required if it is assumed that the motion of the hydrometeor cannot represent atmospheric disturbance. That is, when estimating σ_v-based EDR, the process of applying the EDR correction for each hydrometeor type has to be considered. II) EDR prediction: If it is assumed that hydrometeor motion can represent atmospheric disturbance regardless of hydrometeor type, then this implies that a prediction for radar-based EDR by σ_v and hydrometeor classification algorithm would be possible. Based on the strong correlation between the dendrite type and σ_v identified in this study, it is expected that the area where strong atmospheric turbulence will occur can be predicted. This will be especially helpful to improve flight safety as the potential area of high EDR can be predicted.

5. Summary and Conclusion

This study was conducted to reduce the adverse effects that can be caused by meteorological phenomena caused by disturbances such as shear/turbulence/icing in aircraft operations. Accordingly, it is intended to help provide real-time weather information for safe navigation by utilizing weather radar products. This has been verified from eight precipitation cases with different conditions (precipitation type and season), using the dominant atmospheric characteristics of each hydrometeor type that can be estimated from σ_v to suggest the possibility of the GZ determination. The results from a previous study on this topic (Suh et al., 2023) were verified in this study, and the key results of each

https://doi.org/10.5194/egusphere-2023-947
Preprint. Discussion started: 15 May 2023

GZ with radar dual-pol variables in stratiform precipitation are as follows (Fig. 14).

Firstly, the variation range of Z_{DR} in the DGZ was narrower than that of σ_v. This suggests that although there are significant variations in Z_{DR} due to particle orientation caused by an atmospheric disturbance, the variation of σ_v is more significant. A strong negative relationship between σ_v-Z_{DR} in all DGZ instances allows us to confirm the features in DN where both Z_{DR} and σ_v are strongly influenced. Therefore, σ_v increases as the turbulence becomes stronger (as Z_{DR} decreases) for oblate particles, but the dependence of σ_v according to atmospheric conditions is more prominent than that of Z_{DR}. The irregular particle shape such as DN can explain the negative relationship of Z_{DR}-ρ_{hv}. Moreover, the DGZ has lower ρ_{hv} compared to the NGZ. This indicates that the DN has unstable movement due to aerodynamic features rather than NE due to an irregular shape.

A weak negative relationship of σ_v-Z_{DR} in the NGZ for the all case can be inferred that this is due to the combination of hydrometeors with NE as the major, which negligible influences on σ_v. Theoretically, the variation of σ_v in NE is negligible regardless of v (e.g., Suh et al., 2023). Therefore, the similarity of particle shape (ρ_{hv}) is higher in NGZ and means that aerodynamic properties in NE are relatively more coherent. In cases of negative Z_{DR} where NE might be sufficiently grown, the inverse relationship of σ_v-ρ_{hv} is enhanced. However, the Z_{DR} for each observation case has a positive relationship with σ_v and a negative relationship with that of ρ_{hv} in the NGZ. This implies that the NGZ could have various hydrometeors that came from the upper layer, and these hydrometeors can be formed by their interactions, secondary ice production, (e.g., Field et al., 2017).

Author contributions

Dr. Sung–Ho Suh designed the study. Dr. Sung-Ho Suh and Dr. Woonseon Jung collected the samples and performed the study. Dr. Sung–Ho Suh, Dr. Hong-Il Kim, and Eun-Ho Choi obtained the

https://doi.org/10.5194/egusphere-2023-947
Preprint. Discussion started: 15 May 2023

results and prepared the manuscript with contributions from all the coauthors. Dr. Jung-Hoon Kim examined the results and checked the manuscript. All authors have read and agreed to the published version of the manuscript.

Competing interest

None.

Code/Data availability

The data obtained by YIT in this study are available on request from Korea Meteorological Administration (KMA) and the codes are available on request from Dr. Sung-Ho Suh.

Acknowledgments

This research was supported by the Space Center Development Project (II) of Ministry of Science and ICT (MSIT)

https://doi.org/10.5194/egusphere-2023-947
Preprint. Discussion started: 15 May 2023

References

Andrić, J., Kumjian, M.R., Zrnić, D.S., Straka, J.M., Melnikov, V.M.: Polarimetric signatures above the melting layer in winter storms: An observational and modeling study, J. Appl. Meteorol. Climatol., 52, 682-700, 2013, https://doi.org/10.1175/JAMC-D-12-028.1.

Bechini, R., Baldini, L., Chandrasekar, V.: Polarimetric radar observations in the ice region of precipitating clouds at C-band and X-band radar frequencies, J. Appl. Meteorol. Climatol., 52, 1147-1169, 2013, https://doi.org/10.1175/JAMC-D-12-055.1.

Brewster, K.A. and Zrnić, D.S.: Comparison of eddy dissipation rates from spatial spectra of Doppler velocities and Doppler spectrum widths, J. Atmos. Ocean. Technol., 3, 440-452, 1986, https://doi.org/10.1175/1520-0426(1986)003<0440:COEDRF>2.0.CO;2.

Doviak, R.J.: Doppler radar and weather observations. Courier Corporation, 2006.

Field, P. R., and Coauthors: Secondary ice production: Current state of the science and recommendations for the future, Meteor. Monogr., 58, Amer. Meteor. Soc., 2017, https://doi.org/10.1175/ AMSMONOGRAPHS-D-16-0014.1.

Gent, R. W., Dart, N. P., Cansdale, J. T.: Aircraft icing. Philosophical Transactions of the Royal Society of London. Series A: Mathematical, Phys. Eng. Sci., 358(1776), 2873-2911, 2000, https://doi.org/10.1098/rsta.2000.0689

Giangrande, S.E. and Ryzhkov, A.V.: Estimation of rainfall based on the results of polarimetric echo classification, J. Appl. Meteorol. Climatol., 47, 2445-2462, 2008, https://doi.org/10.1175/2008JAMC1753.1.

Gourley, J. J., Tabary, P., and Du Chatelet, J. P.: A fuzzy logic algorithm for the separation of precipitating from nonprecipitating echoes using polarimetric radar observations, J. Atmos. Ocean Technol., 24, 1439-1451, 2007, https://doi.org/10.1175/JTECH2035.1.

Hashino, T., Chiruta, M., Polzin, D., Kubicek, A., Wang, P.K.: Numerical simulation of the flow fields around falling ice crystals with inclined orientation and the hydrodynamic torque, Atmos. Res. 150, 79-96, 2014, https://doi.org/10.1016/j.atmosres.2014.07.003.

Hashino, T., K.-Y. Cheng, C.-C. Chueh, and P. K. Wang: Numerical study of motion and stability of falling columnar crystals, J. Atmos. Sci., 73, 1923-1942, 2016, https://doi.org/10.1175/JAS-D-15-0219.1.

Hocking, W. K.: Measurement of turbulent energy dissipation rates in the middle atmosphere by radar techniques: A review, Radio Sci., 20, 1403-1422, 1985, https://doi.org/10.1029/RS020I006P01403.

Istok, M.J., Doviak, R.J.: Analysis of the relation between Doppler spectral width and thunderstorm turbulence, J. Atmos. Sci,. 43, 2199-2214, 1986, https://doi.org/10.1175/1520-0469(1986)043<2199:AOTRBD>2.0.CO;2.

Jacoby-Koaly, S., and Coauthors: Turbulent dissipation rate in the boundary layer via UHF wind profiler Doppler spectral width measurements, Boundary Layer Meteorol., 103, 361-389, 2002, https://doi.org/10.1023/A:1014985111855.

Ji, W., Wang, P.K.: Numerical simulation of three-dimensional unsteady viscous flow past finite cylinders in an unbounded fluid at low intermediate Reynolds numbers, Theor. Comput. Fluid Dyn., 3, 43-59, 1991, https://doi.org/10.1007/BF00271515.

https://doi.org/10.5194/egusphere-2023-947
Preprint. Discussion started: 15 May 2023

Kennedy, P.C. and Rutledge, S.A.: S-band dual-polarization radar observations of winter storms, J. Appl. Meteorol. Climatol., 50, 844-858, 2011, https://doi.org/10.1175/2010JAMC2558.1.

Kim, J.-H., Park, J.-R., Kim, S.-H., Kim, J., Lee, E., Baek, S., and Lee, G.: A detection of convectively induced turbulence using in situ aircraft and radar spectral width data, Remote Sens., 13, 726, 2021, https://doi.org/10.3390/rs13040726.

Knupp, K.R. and Cotton, W.R.: An intense, quasi-steady thunderstorm over mountainous terrain. Part II: Doppler radar observations of the storm morphological structure, J. Atmos. Sci., 39, 343-358, 1982, https://doi.org/10.1175/1520-0469(1982)039<0343:AIQSTO>2.0.CO;2.

Labitt, M.: Coordinated radar and aircraft observations of turbulence. Massachusetts Inst. of Tech. Lexington Lincoln Lab, 1981.

Libbrecht, K. G.: Ken Libbrecht's field guide to snowflakes. Voyageur Press, 2006.

List, R., Schemenauer, R.S.: Free-fall behavior of planar snow crystals, conical graupel and small hail, J. Atmos. Sci., 28, 110-115, 1971, https://doi.org/10.1175/1520-0469(1971)028<0110:FFBOPS>2.0.CO;2.

Mason, B., 1971: The Physics of Clouds. Clarendon Press.

Melnikov, V. M., and Doviak, R. J.: Turbulence and wind shear in layers of large Doppler spectrum width in stratiform precipitation, J. Atmos. Ocean Technol., 26, 430-443, 2009, https://doi.org/10.1175/2008JTECHA1108.1.

Nakaya, U. and Terada Jr, T.: Simultaneous observations of the mass, falling velocity and form of individual snow crystals, J. the Faculty of Sci., Hokkaido Imperial Univ., 1, 191-200, 1935, http://hdl.handle.net/2115/34452.

Politovich, M. K.: Aircraft icing. Encyclopedia of Atmos. Sci., 358(1776), 68-75, 2003.

https://doi.org/10.5194/egusphere-2023-947
Preprint. Discussion started: 15 May 2023

Ribaud, J. F., Bousquet, O., and Coquillat, S.: Relationships between total lightning activity, microphysics and kinematics during the 24 September 2012 HyMeX bow-echo system, Q. J. R. Meteorol. Soc., 142, 298-309, 2016, https://doi.org/10.1002/qj.2756.

Ryzhkov, A., Zhang, P., Reeves, H., Kumjian, M., Tschallener, T., Trömel, S., Simmer, C.: Quasi-vertical profiles—A new way to look at polarimetric radar data, J. Atmos. Ocean. Technol., 33, 551-562, 2016, https://doi.org/10.1175/JTECH-D-15-0020.1

Ryzhkov, A. V., Giangrande, S. E., Melnikov, V. M., Schuur, T. J.: Calibration issues of dual-polarization radar measurements, J. Atmos. Ocean Technol., 22(8), 1138-1155, 2005, https://doi.org/10.1175/JTECH1772.1.

Ryzhkov, A.V., Zrnić, D., Gordon, B.: Polarimetric method for ice water content determination, J. Appl. Meteorol., 37, 125-134, 1998, https://doi.org/10.1175/1520-0450(1998)037<0125:PMFIWC>2.0.CO;2.

Suh, S.-H., Choi, E.-H., Kim, H.-I., and Jung, W.: Possibility of Solid Hydrometeor Growth Zone Identification Using Radar Spectrum Width. Adv. Atmos. Sci., 40, 317-332, 2023, https://doi.org/10.1007/s00376-022-1472-0.

Trömel, S., Ryzhkov, A. V., Hickman, B., Mühlbauer, K., and Simmer, C.: Polarimetric radar variables in the layers of melting and dendritic growth at X band—Implications for a nowcasting strategy in stratiform rain, J. Appl. Meteorol. Climatol., 58(11), 2497-2522, 2019, https://doi.org/10.1175/JAMC-D-19-0056.1.

Vivekanandan, J., Bringi, V.N., Hagen, M., Meischner, P.: Polarimetric radar studies of atmospheric ice particles. EEE Trans. Geosci. Remote Sens., 32, 1-10, 1994, https://doi.org/10.1109/36.285183.

https://doi.org/10.5194/egusphere-2023-947
Preprint. Discussion started: 15 May 2023

Wang, P.K. and Ji, W.: Numerical simulation of three-dimensional unsteady flow past ice crystals, J. Atmos. Sci., 54, 2261-2274, 1997, https://doi.org/10.1175/1520-0469(1997)054<2261:NSOTDU>2.0.CO;2.

Wang, P.K. and Ji, W.: Collision efficiencies of ice crystals at low–intermediate Reynolds numbers colliding with supercooled cloud droplets: A numerical study, J. Atmos. Sci., 57, 1001-1009, 2000, https://doi.org/10.1175/1520-0469(2000)057<1001:CEOICA>2.0.CO;2.

Wang, P.K.: Ice microdynamics, Elsevier, 2002.

Williams, E., Smalley, D., Donovan, M., Hallowell, R., Hood, K., Bennett, B., Evaristo, R., Stepanek, A., Bals-Elsholz, T., and Cobb, J.: Dual polarization radar winter storm studies supporting development of NEXRAD-based aviation hazard products, AMS 35th Conf. on Radar Meteorol., Pittsburgh, 26-30, 2011.

Williams, E., Smalley, D., Donovan, M., Hallowell, R., Hood, K., Bennett, B., Wolde, M., Bastian, M., Korolev, A.: Validation of NEXRAD radar differential reflectivity in snowstorms with airborne microphysical measurements: Evidence for hexagonal flat plate crystals, 36th Conf. on Radar Meteorol, 2013.

Willmarth, W.W., Hawk, N.E., Harvey, R.L.: Steady and unsteady motions and wakes of freely falling disks, Phys., Fluids, 7, 197-208, 1964, https://doi.org/10.1063/1.1711133.

Wolde, M., Vali, G.: Polarimetric signatures from ice crystals observed at 95 GHz in winter clouds. Part I: Dependence on crystal form, J. Atmos. Sci., 58, 828-841, 2001, https://doi.org/10.1175/1520-0469(2001)058<0828:PSFICO>2.0.CO;2.

https://doi.org/10.5194/egusphere-2023-947
Preprint. Discussion started: 15 May 2023

Zhang, P., Chan, P., Doviak, R., Fang, M.: Estimate of Eddy Dissipation Rate Using Spectrum Width Observed by the Hong Kong TDWR Radar. 34th Conf. on Radar Meteorol., 2009, https://ams.confex.com/ams/34Radar/techprogram/paper_155531.htm.

Tables

Table 1. Specifications of Yongin Testbed (YIT).

Specifications	Details
Model	DWSR-8501 S/K-SDP
Manufacturer	EEC (US)
Transmitting tube	Klystron
Antenna diameter	8.5 m
Transmission frequency	2.88 GHz
Peak power	850 KW
Effective observation range	240 km
Beam / Pulse width	0.94° / 2 µs
Wavelength	10.41 cm
Range gate size	250 m
Elev. height	473 m
Long. / Lat.	127.2852 °E / 37.2063 °N
Obs. interval	10 min

https://doi.org/10.5194/egusphere-2023-947
Preprint. Discussion started: 15 May 2023

523 **Table 2.** Information of precipitation cases selected in this study.

No	Case	Date	Time (LST)	θ for QVP	Type	Season
1	SW1	16. Feb. 2015	0000-0600	16.4	Stratiform	Winter
2	SW2	21. Feb. 2015	1000-1700	16.4	Stratiform	Winter
3	SW3	27. Feb. 2016	0000-0600	19.0	Stratiform	Winter
4	SW4	28. Feb. 2016	1200-1900	19.0	Stratiform	Winter
5	CP5	02. May. 2016	1800-2400	17.3	Convective	Spring
6	CP6	10. May. 2016	0600-1500	17.3	Convective	Spring
7	SP7	24. May. 2016	0330-1100	17.3	Stratiform	Spring
8	CS8	01. Jul. 2016	1330-1630	17.3	Convective	Summer

https://doi.org/10.5194/egusphere-2023-947
Preprint. Discussion started: 15 May 2023

Figures

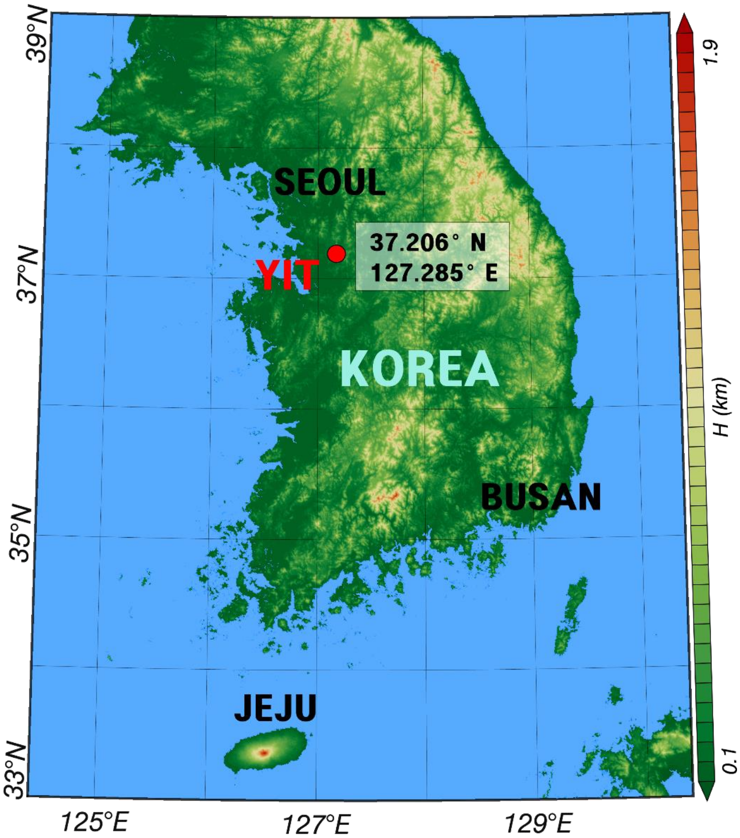

Figure 1. Origin of Yongin Testbed (YIT) dual-pol weather radar data (red bullet) in South Korea.

https://doi.org/10.5194/egusphere-2023-947
Preprint. Discussion started: 15 May 2023

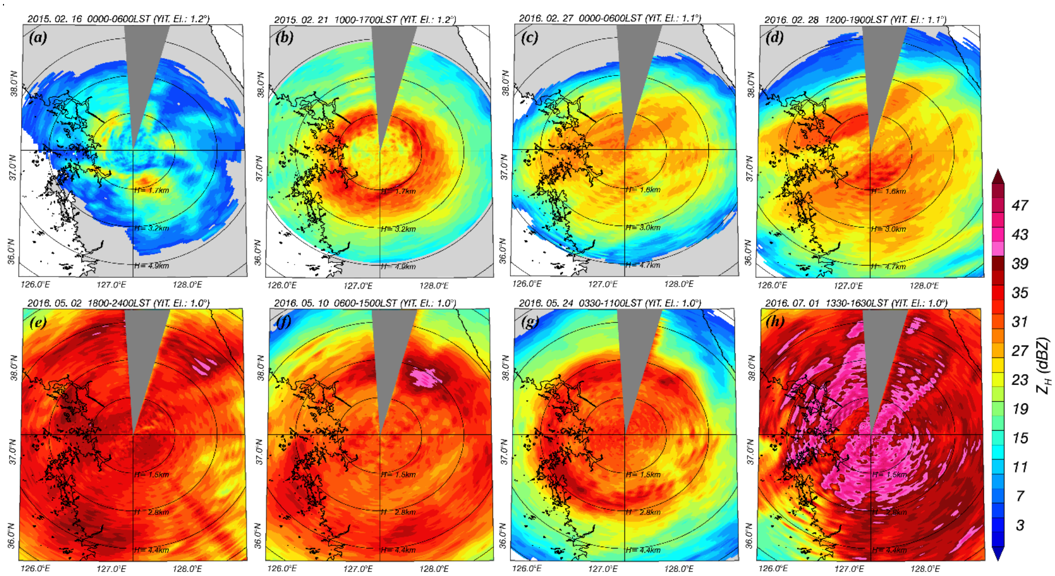

Figure 2. Cumulate maximum Z_H in PPI at the lowest elevation angle for analysis cases. The grey blank indicates a beam blockage area. The range rings are centered on the YIT radar at 50 km.

https://doi.org/10.5194/egusphere-2023-947
Preprint. Discussion started: 15 May 2023

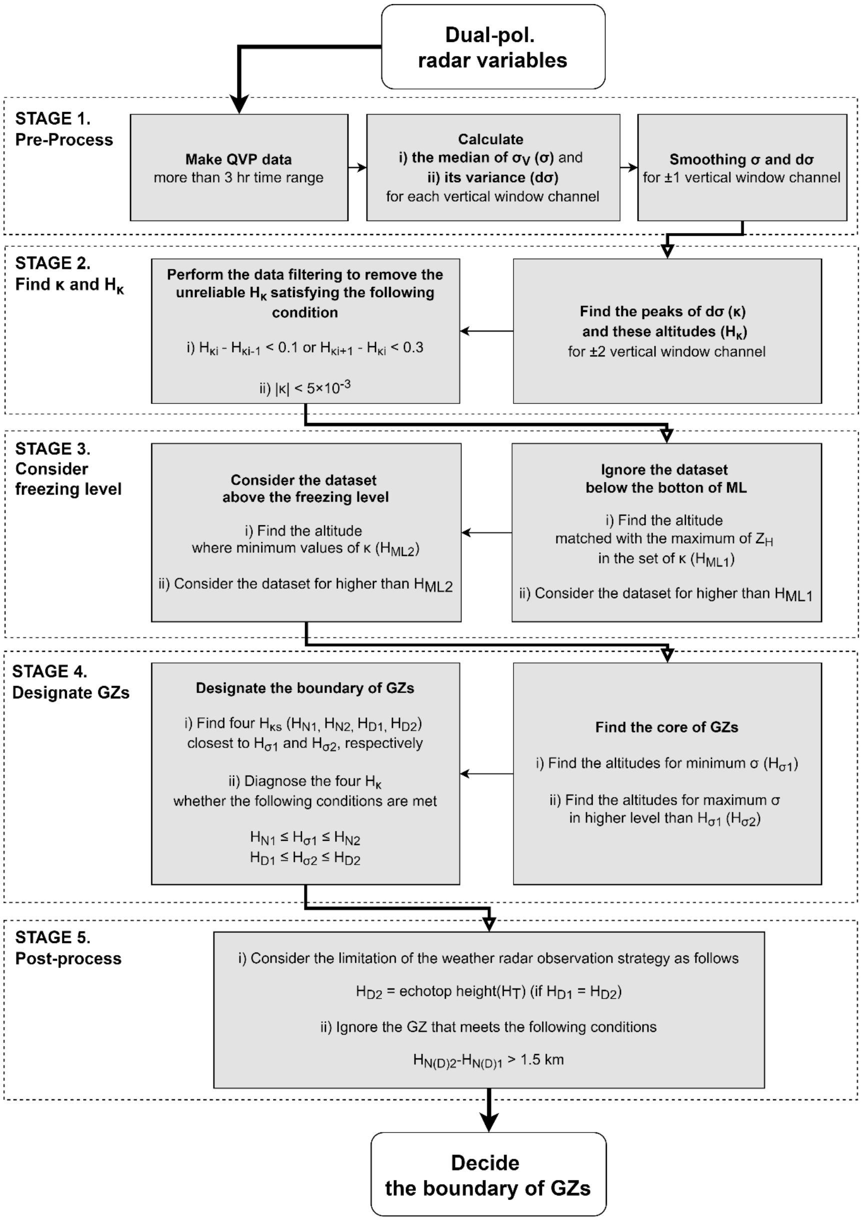

Figure 3. The algorithm of GZDA.

https://doi.org/10.5194/egusphere-2023-947
Preprint. Discussion started: 15 May 2023

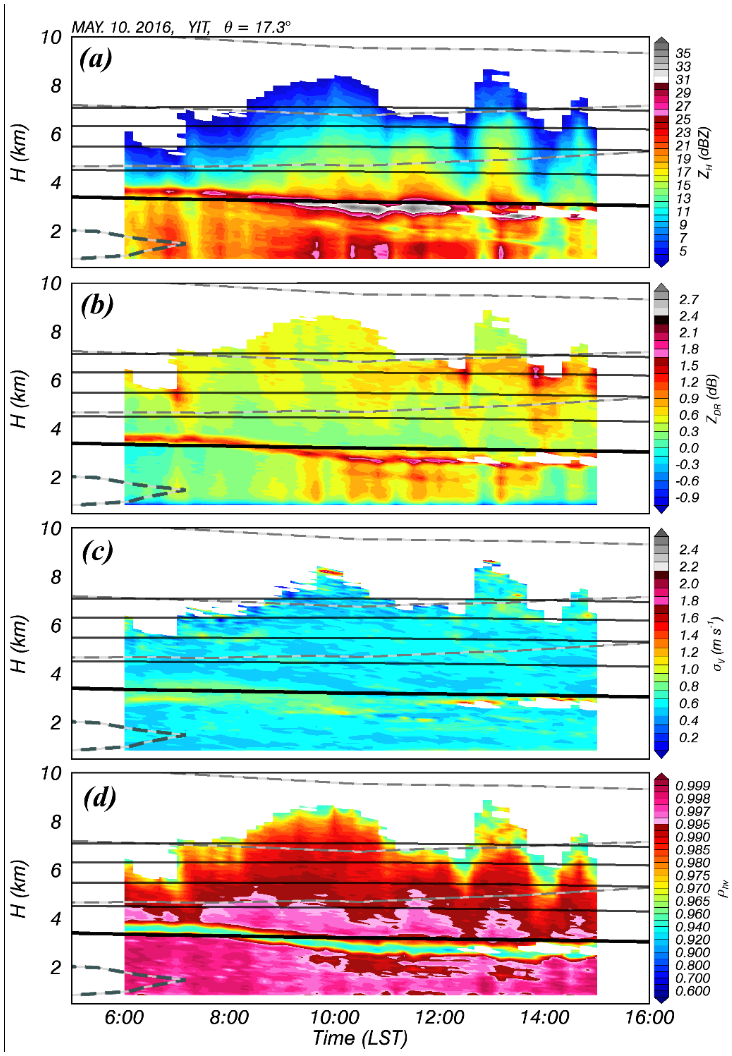

Figure 4. QVP of (a) Z_H, (b) Z_{DR}, (c) σ_v, and (d) ρ_{hv} in the representative non-winter precipitation (10th May 2016). Solid black and dashed blue curves in the background represent T and *v*, respectively, obtained from the MSM reanalysis data. The temperature profile is expressed down to -20ºC.

https://doi.org/10.5194/egusphere-2023-947
Preprint. Discussion started: 15 May 2023

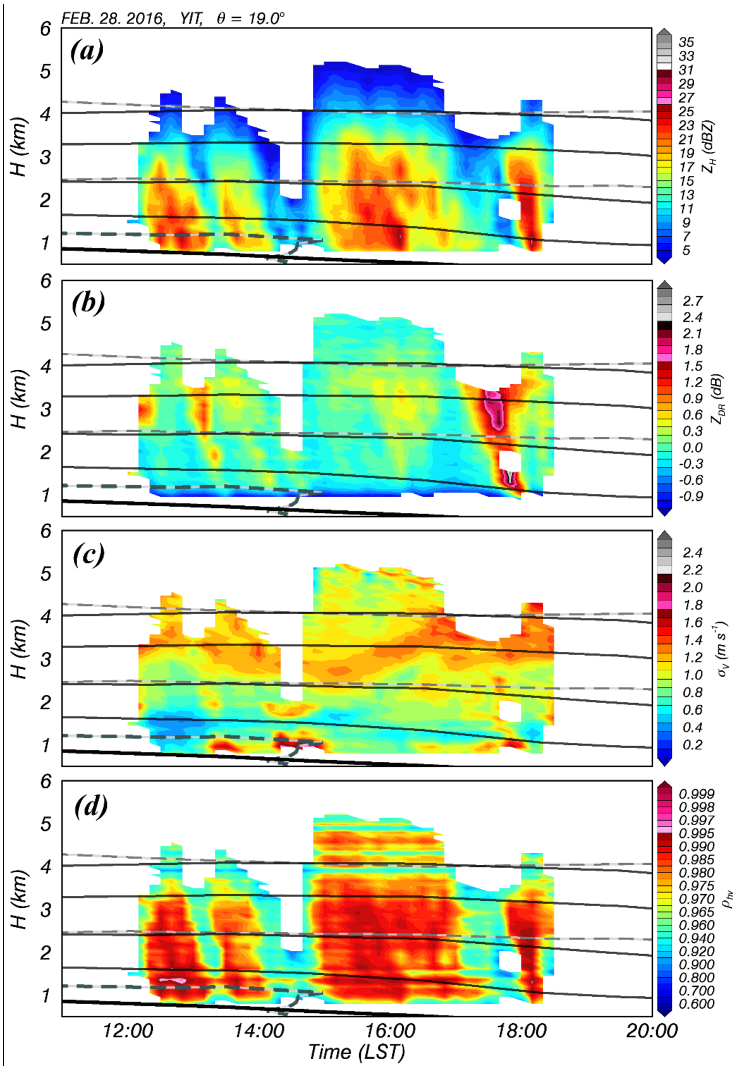

Figure 5. Symbols and colors are the same as in Figure 4 but for the representative winter precipitation (28th Feb 2016).

.

https://doi.org/10.5194/egusphere-2023-947
Preprint. Discussion started: 15 May 2023

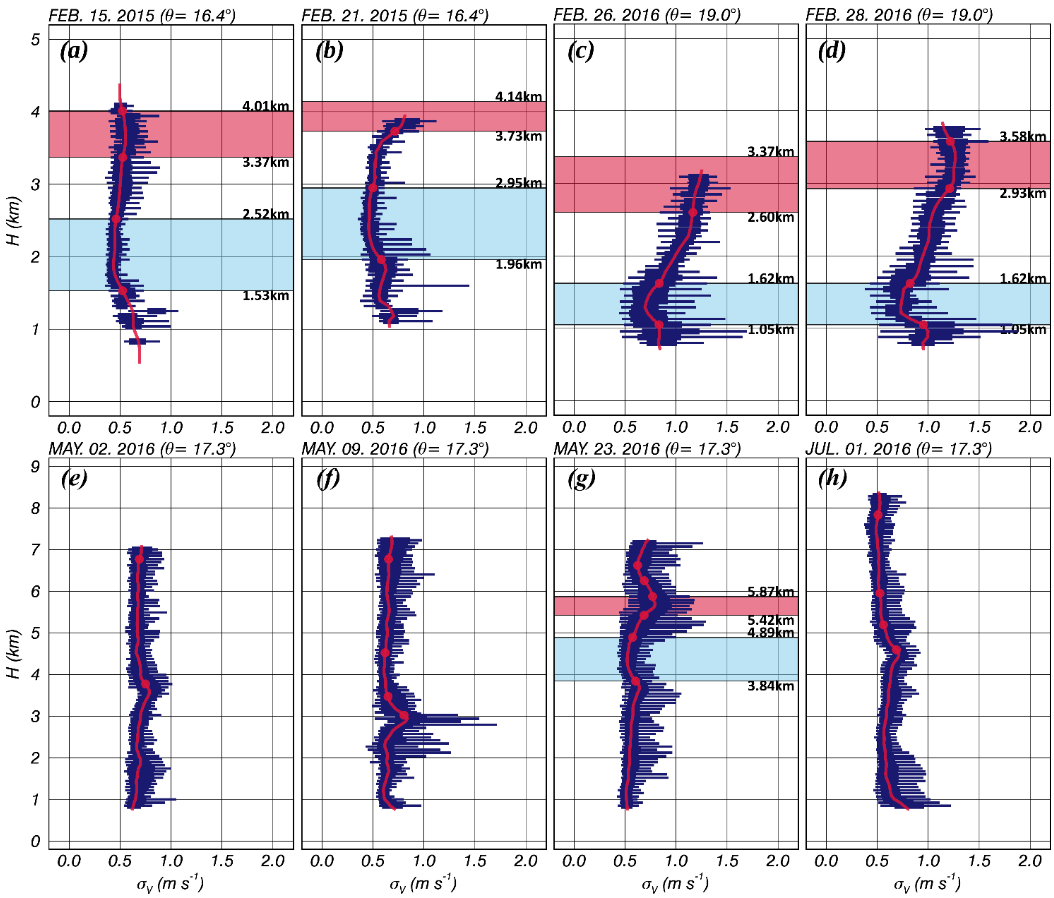

Figure 6. Vertical profiles of σ_v quartiles for each height resolution level. The solid red lines indicate averaged σ_v values, while red circles represent the peak point of $d\sigma_v$. Red and blue shaded areas are the areas of the DGZ and the NGZ, respectively, as determined by GZDA.

https://doi.org/10.5194/egusphere-2023-947
Preprint. Discussion started: 15 May 2023

553

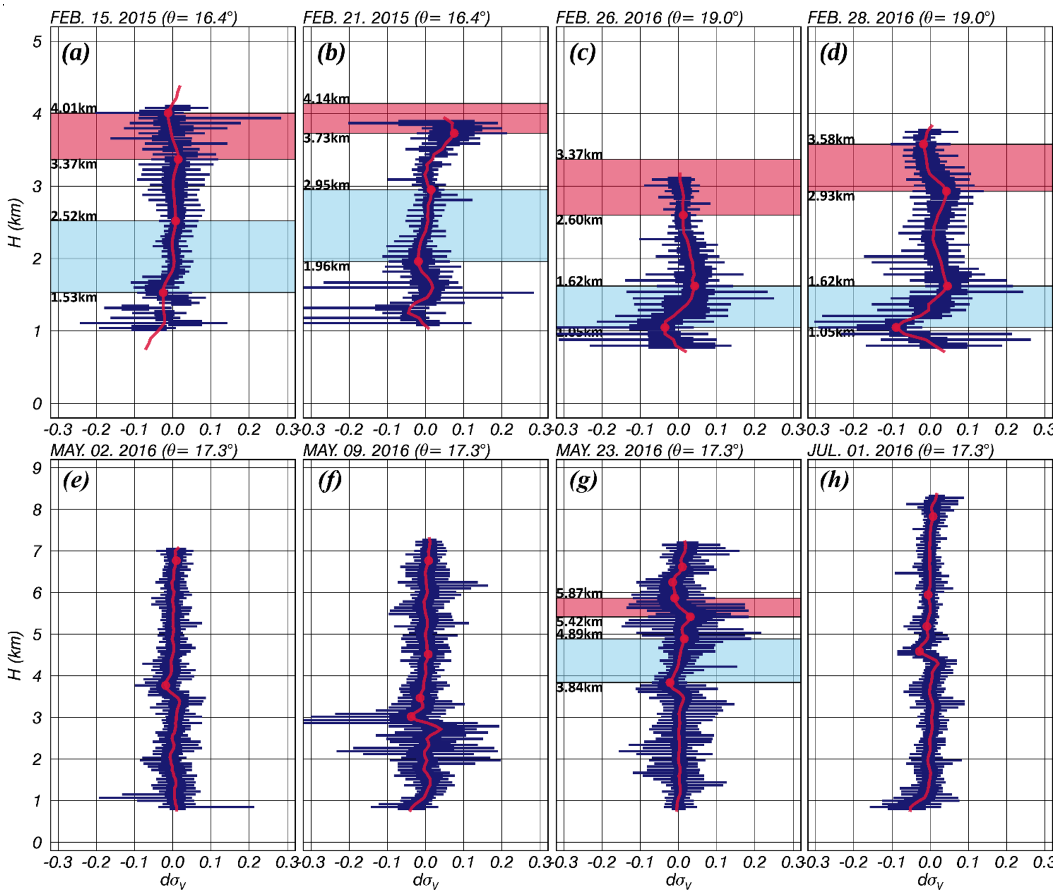

554

555 Figure 7. Symbols and colors are the same as in Figure 6 but for the $d\sigma_v$.

556

https://doi.org/10.5194/egusphere-2023-947
Preprint. Discussion started: 15 May 2023

557 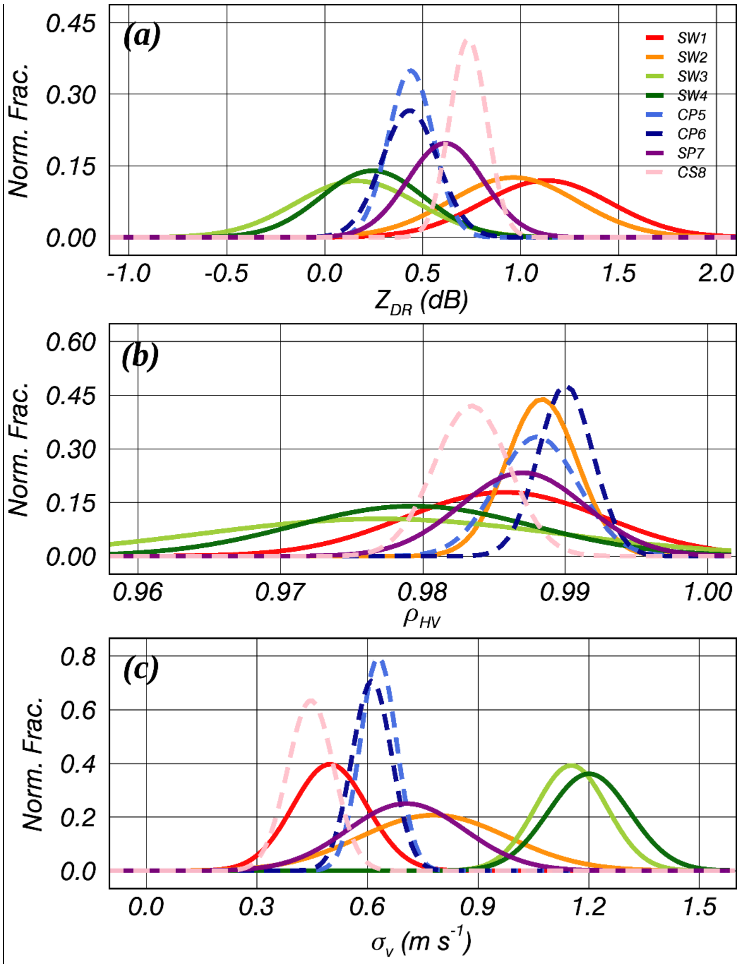

558 Figure 8. Normalized Gaussian distribution of (a) Z_{DR}, (b) ρ_{hv}, and (c) σ_v in the DGZ for analyzed
559 cases. The solid and broken line represents stratiform and convective types, respectively.

560

https://doi.org/10.5194/egusphere-2023-947
Preprint. Discussion started: 15 May 2023

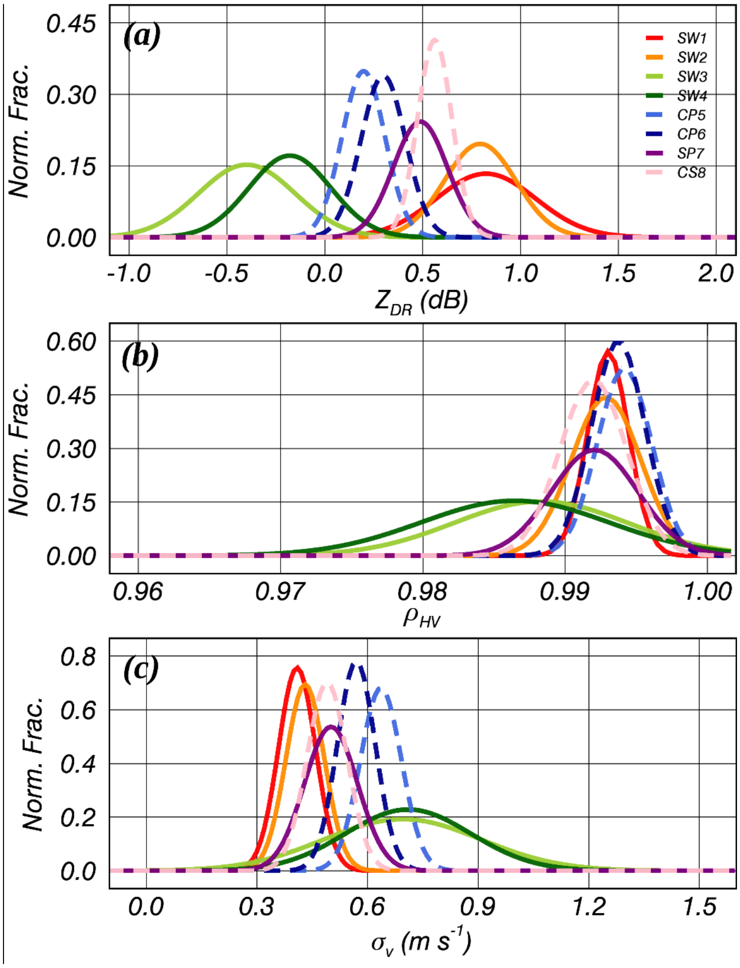

Figure 9. Legend is the same as in Figure 8 but for the NGZ.

https://doi.org/10.5194/egusphere-2023-947
Preprint. Discussion started: 15 May 2023

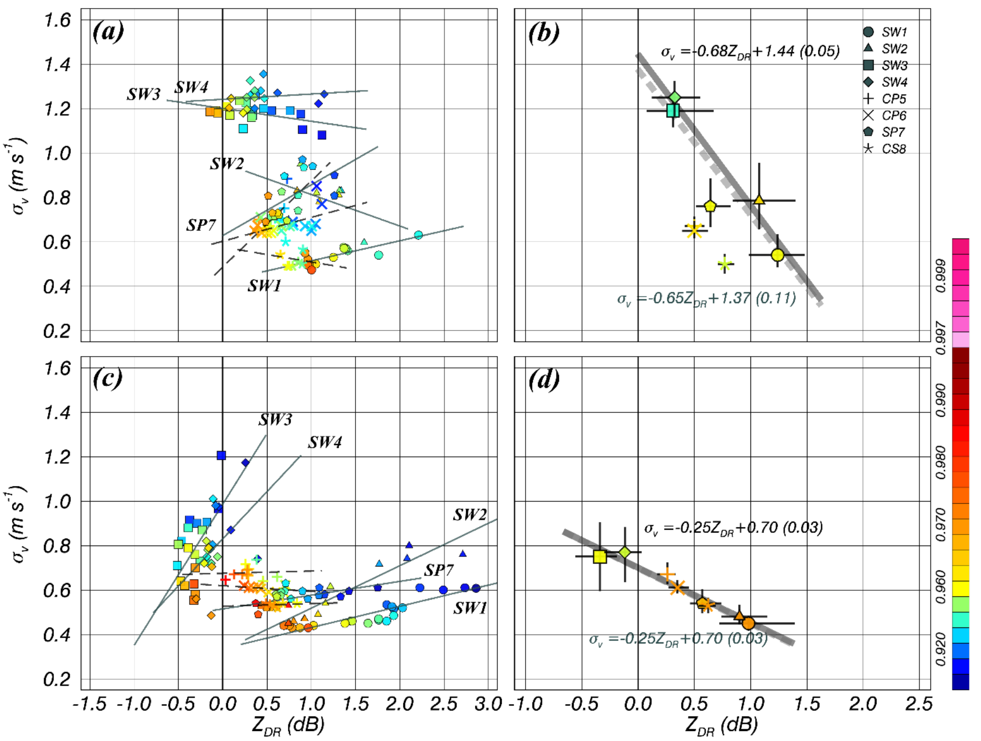

Figure 10. Scatter plot of the averaged σ_v –Z_{DR} by rank of ρ_{hv} for the DGZ (a & b) and the NGZ (c & d). The σ_v –Z_{DR} were averaged (a & c) within each case and for each case (b & d), respectively. Solid lines represent a regression line, and the shape of crosses overlapped with each symbol in (b & d) indicate the 1st to 3rd quartiles for variables on each axis. Thick solid and broken lines represent a regression line for the winter and whole stratiform cases, respectively. The parentheses in relationships are the RMSE.

https://doi.org/10.5194/egusphere-2023-947
Preprint. Discussion started: 15 May 2023

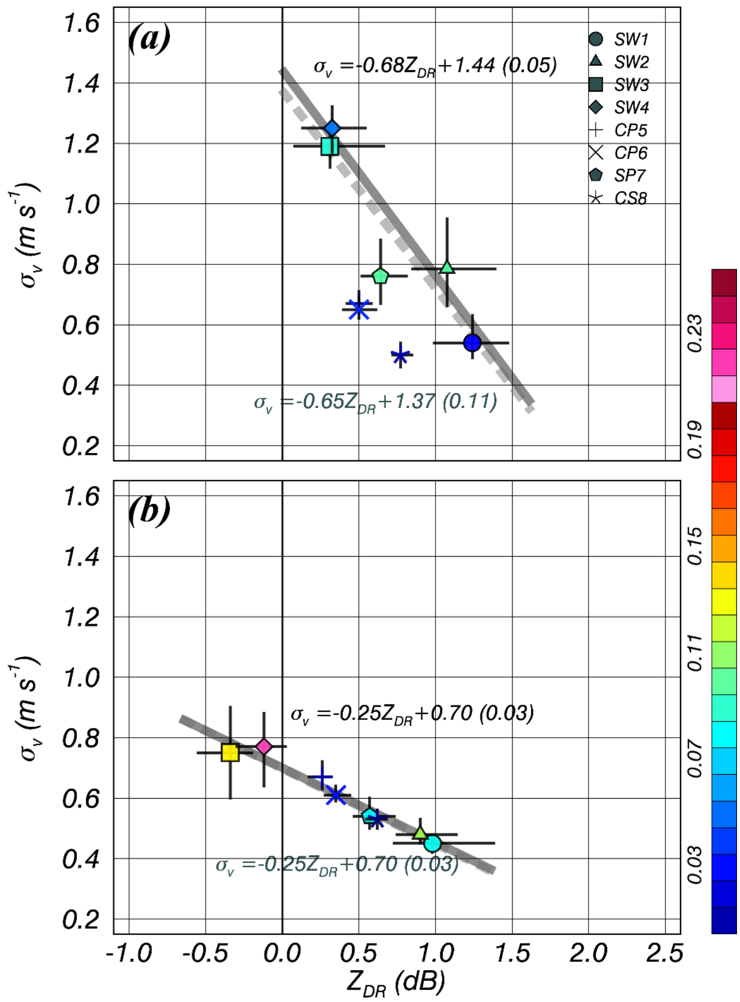

Figure 11. Scatter plot of the averaged σ_v –Z_{DR} for the case in (a) the DGZ and (b) the NGZ. The colors on the symbols represent the $d\sigma_{MAX}$. Thick solid and broken lines represent a regression line for the winter and whole stratiform cases, respectively. The shape of crosses overlapped with each symbol indicates the 1st to 3rd quartiles for variables on each axis. The parentheses in relationships are the RMSE.

https://doi.org/10.5194/egusphere-2023-947
Preprint. Discussion started: 15 May 2023

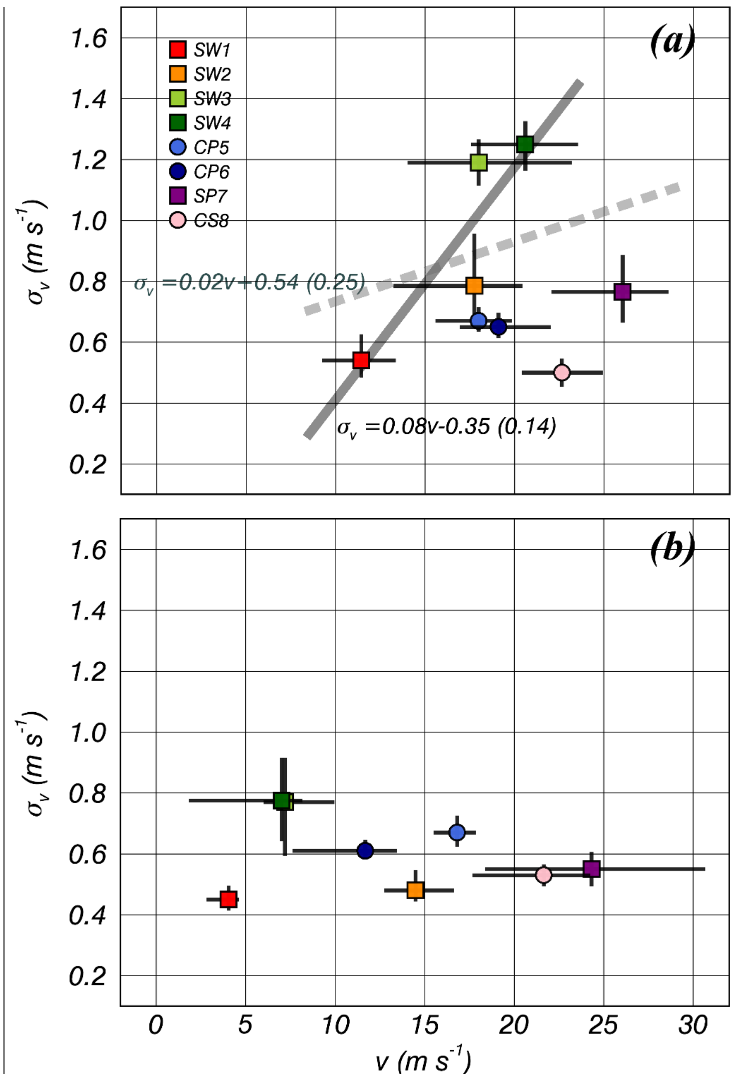

Figure 12. Scatter plot of the averaged σ_v – *v* for the case in (a) the DGZ and (b) the NGZ. The colors of the symbol represent the case. Thick solid and broken lines represent a regression line for the winter and whole stratiform cases, respectively. The shape of crosses overlapped with each symbol indicates the 1st to 3rd quartiles for variables on each axis. The parentheses in relationships are the RMSE.

https://doi.org/10.5194/egusphere-2023-947
Preprint. Discussion started: 15 May 2023

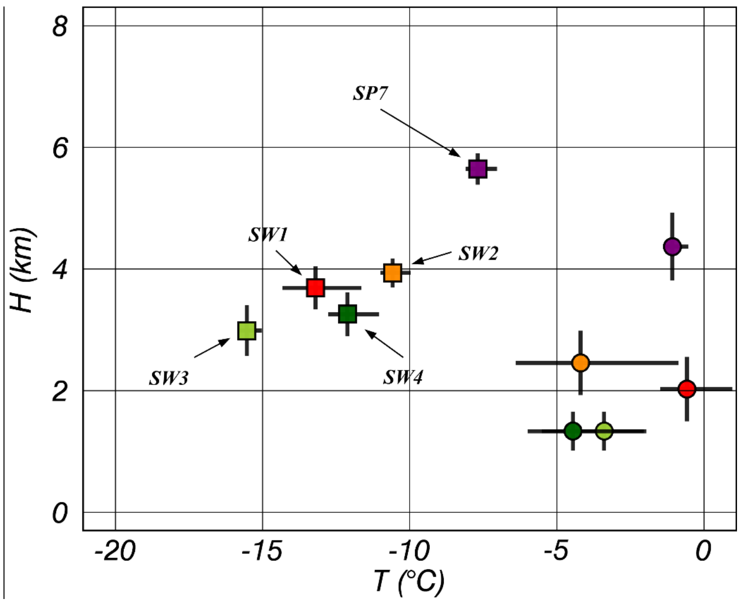

Figure 13. Scatter plot of the averaged H–T for the stratiform case in the DGZ (square symbols) and the NGZ (circle symbols). The colors on the symbol represent the case. The shape of crosses overlapped with each symbol indicates the 1st to 3rd quartiles for variables on each axis.

https://doi.org/10.5194/egusphere-2023-947
Preprint. Discussion started: 15 May 2023

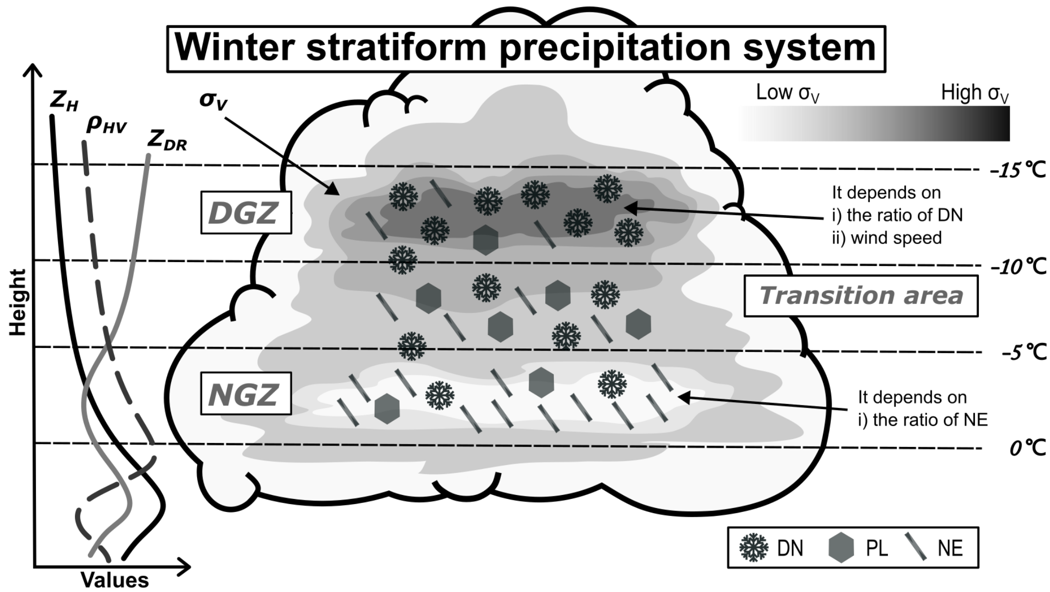

Figure 14. Schematic representation of the vertical structure of radar variables and the expected distribution of solid hydrometeors in a stratiform precipitation system above the melting layer.